$2s$-$2p$ transitions in heliumlike and lithiumlike krypton

S. Martin, A. Denis, M. C. Buchet-Poulizac, J. P. Buchet, and J. Désesquelles
Laboratoire de Spectrométrie Ionique et Moléculaire, Université Claude Bernard (Lyon 1), 43 Bd. du 11 Novembre 1918, 69622 Villeurbanne CEDEX, France
(Received 12 March 1990; revised manuscript received 31 May 1990)

We present a study of the $1s2s\,{}^3S_1$–$1s2p\,{}^3P_{0,2}$ transitions in Kr^{34+} and the $1s^22s\,{}^2S_{1/2}$–$1s^22p\,{}^2P_{1/2,3/2}$ transitions in Kr^{33+}. Wavelengths of two- and three-electron krypton ions have been accurately measured using the beam-foil technique. The limits of precision are discussed. Our results are compared with Z-expansion and multiconfigurational Dirac-Fock theories taking account of the two-electron quantum electrodynamics (QED) contributions we have calculated for high-Z ions. The agreement is satisfactory for heliumlike Kr XXXV. However, a sizable disagreement is found for the $2p\,{}^2P_{1/2}$–$2p\,{}^2P_{3/2}$ fine structure of lithiumlike Kr XXXIV, which could reflect the difficulty of calculating the QED corrections and retarded Breit interactions for three-electron ions.

I. INTRODUCTION

The atomic structure of two- and three-electron ions has been a subject of intense research interest during recent years. In recent papers of Drake,[1] Hata and Grant,[2] and Indelicato, Gorceix, and Desclaux[3] on two-electron ion structure, the Breit interaction, the correlation energy, and the quantum electrodynamics (QED) corrections are taken into account precisely. Interest in the structure of $n=2$ levels of high-Z heliumlike ions is due to increased importance of the one-electron QED contributions which scale roughly like Z^4 compared to the two-electron QED correction which varies approximately as Z^3. Unfortunately wavelengths for two-electron ions of nuclear charge Z greater than 18 have not yet been measured very precisely, mainly for lack of available intense light sources.

The many-body perturbation theory (MBPT) has been used by Lindgren[4] for lithium atoms and by Johnson, Blundell, and Sapirstein[5] for three-electron ions from $Z=3$ up to $Z=92$. The multiconfigurational Dirac-Fock theory (MCDF) including high-order correlation energies has been applied by Indelicato[6] to several lithiumlike ions. QED effects are as important for three-electron ions as for two-electron ions and are evidently more difficult to calculate.

In this paper we mainly concern ourselves with the $2s\,{}^3S_1-2p\,{}^3P_2$ and $2s\,{}^3S_1-2p\,{}^3P_0$ transitions in heliumlike krypton ($Z=36$) and the $2s\,{}^2S_{1/2}-2p\,{}^2P_{1/2,3/2}$ transitions in lithium krypton. We had published a measurement of the heliumlike $1s2s\,{}^3S_1-1s2p\,{}^3P_2$ transition in a previous Brief Report.[7] The wavelength was measured at 111.15 ± 0.08 Å. Now, after having improved our detection system and using new techniques of ion excitation, we are able to give a more precise result. The new wavelength is 111.11 ± 0.03 Å. Wavelengths measured in lithiumlike Kr XXXIV at 91.00 ± 0.03 Å and 173.93 ± 0.04 Å correspond to the $1s2s\,{}^2S_{1/2}-1s2p\,{}^2P_{3/2}$ and $-1s2p\,{}^2P_{1/2}$ transitions, respectively. The deduced $1s^22p\,{}^2P_{3/2}-{}^2P_{1/2}$ fine structure is $523\,957\pm300$ cm.$^{-1}$ Denne and Hinnov[8] have measured these wavelengths in a tokamak source obtaining values different from ours. Disagreements are discussed in Sec. VI. Krypton is the highest system for which measurements of $2s$-$2p$ transition energies have been performed in both the two- and three-electron isoelectronic sequences with a sufficient accuracy to be sensitive to high-order contributions and to test calculations.

II. EXPERIMENT

A. Experimental arrangement

The setup is slightly different from that of Martin *et al.*[7] In the present experiment, ions accelerated by the Grand Accélérateur National d'Ions Lourds (GANIL) at Caen, France, were directed through an excitation foil after having passed by the Ligne d'Ions Super Epluchés (LISE) facility, where they are stripped and analyzed for charge-state properties. Charge-state distributions are presented in Fig. 1 from a 34.4224-MeV/amu $^{84}Kr^{26+}$ beam passing through various carbon foils. Outgoing krypton charges are available from 26+ to 36+. Typical particle currents on target were 400 nA. A dozen excitation foils were mounted on an adjustable carriage.

A 2.2-m grazing-incidence MacPherson 247 monochromator was set at $90.68°\pm0.04°$ to the beam direction. Its 600-groove/mm platinum-coated grating was blazed at 116 Å (86° incidence angle). A position-sensitive detector was located at the focal plane in place of the monochromator exit slit. More details on this detection were given in Martin, Druetta, and Désesquelles.[9] Pulses from the position calculator were sent into a 2048-channel Nucleus analog-to-digital convertor (ADC) card placed in an Apple II microcomputer. Galileo multichannel plates (MCP) were adjusted on the Rowland circle by an X,Y,θ Micro Controle micrometer movement. Resolution was better than 0.2 Å when using a 5-μm entrance slit.

 ©1990 The American Physical Society

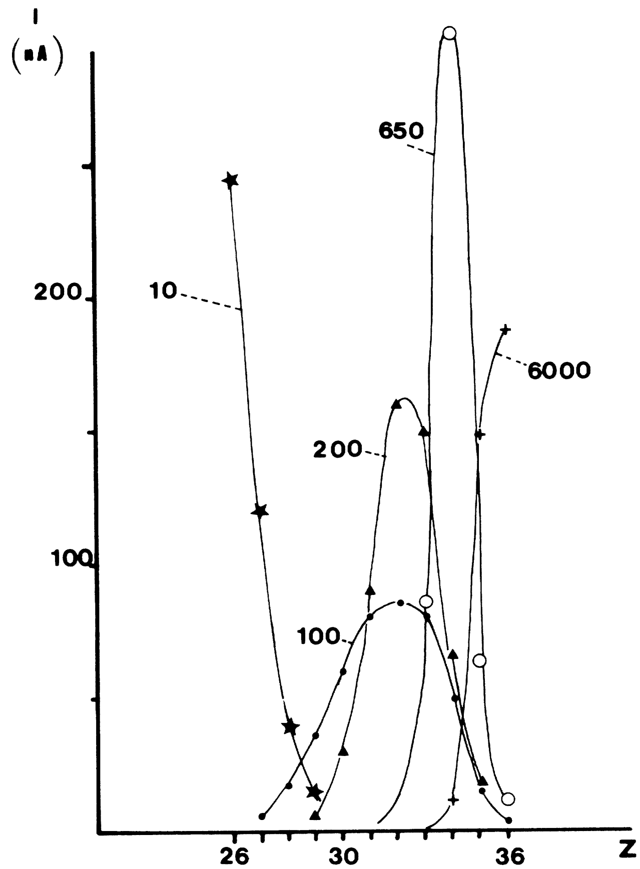

FIG. 1. Charge-state distribution measured for 35-MeV/u Kr^{26+} projectiles transmitted through carbon foils of 10, 100, 200, 650, and 6000 $\mu g/cm^2$ thickness.

B. Spectrometer calibration

The dispersion curve of the monochromator has been determined using a Penning gauge located in front of the entrance slit. Many lines observed from 240 to 700 Å in He I, He II, Ne I, and Ne II were selected as wavelength standards.

The static calibration of the position-sensitive detector was obtained in two successive steps. First the center of the MCP was calibrated all along the Rowland circle. Accuracy of the adjustment is about 0.01 Å. In a second step the dispersion of the standard lines was calibrated for a given position of the detector. We found that the linearity of the anode encoder edges is not good. In consequence we used only a 10-mm-wide part out of the 25 mm available on the detector to ensure a ± 0.01-Å accuracy. Finally the dispersion corrected wavelength becomes

$$\lambda = \frac{1}{kN}\{\sin\alpha - \sin[\arccos(Y/R) \pm A]\} ,$$

where

$$A = \arccos\left[\frac{Y + X\cos B}{(Y^2 + X^2 + 2YX\cos B)^{1/2}}\right] .$$

The + (−) sign corresponds to $x < 0$ ($x > 0$). α is the incidence angle, N the number of lines of the grating, R the radius, k the order of diffraction, Y the distance from the center of the MCP to the center of the grating, X the distance from the center of the MCP to the position on the MCP,

$$B = \frac{\pi}{2} - \arccos\frac{Y}{R} + B' ,$$

and B' is the angle between the Rowland circle and the MCP plane. α, R and B' are determined by minimizing the difference to the calibration lines.

C. Doppler-Fizeau shift

Because the Doppler-Fizeau effect shifts lines emitted by fast particles, it has been necessary either to use in-beam foil-excited lines as references or to know the beam velocity and the observation angle precisely. To this end two methods have been employed.

First, transitions between Rydberg states of Kr XXXIV and Kr XXXV have been used as their energies can be accurately calculated in lithium and helium sequences. However, a low uncertainty was introduced by the model of level populations we chose and corrections were needed to take account of the dependence of line centroids and shapes on the way the grating is illuminated and consequently on the lifetime of upper levels.[10]

Second, the incident-beam velocity, the energy loss in the carbon foil, and the observation angle have been measured precisely. The incident-beam velocity was given by a magnetic spectrometer with a 2×10^{-4} relative precision corresponding to $\Delta\lambda = 0.001$ Å at 100 Å. The energy loss in 1 mg/cm^2 carbon target has been deduced from Bimbot's tables[11] to be 16.3 MeV at 35 MeV/u. A 10% error on this value corresponds to an error in wavelength of 0.002 Å at 100 Å. The observation window has been determined using a lamp and a slit moving parallel to the ion beam at about 5 m in front of the spectrometer working at zeroth order. Photons were detected behind the exit slit by a photomultiplier. We have verified that the observation window is found to be similar when using an uv light source which was a Penning discharge inside the pumped target chamber. Only the rising and falling slopes were different. The reference axis at 90° has been obtained by using a 90° prism with an accuracy of $\pm 3''$. The observation angle has been determined before and after the krypton wavelength measurements at $90.68\pm 0.04°$. Uncertainty corresponds to $\Delta\lambda = 0.019$ Å at $\lambda = 100$ Å. During the fast ion wavelength measurements, the ion beam position was fixed on a grid at about 5 m downstream of the foil allowing the calculation of angle corrections on measured wavelengths.

III. PRODUCTION OF EXCITED STATES IN GIVEN CHARGE STATES

Light intensity dependence upon foil thickness and incoming ion charge has been studied for several transitions of various outgoing charge states. Results are displayed in Fig. 2(a) for the Kr XXXIV $1s^22s\ ^2S_{1/2}$ −

$1s^2 2p\ ^2P_{3/2}$ transition. The foil thickness was inside the 10–6000 $\mu g/cm^2$ range and the incoming charge was 32+, 33+, or 34+. The highest intensity was obtained with an incoming Kr^{33+} beam and a 80 $\mu g/cm^2$ carbon foil. Half this maximum was given by a 10 $\mu g/cm^2$ target.

A similar study has been made for the $1s^2 2s^2\ ^1S_0 - 1s^2 2s2p\ ^1P_1$ and $1s^2 2s2p\ ^3P_0 - 1s^2 2p^2\ ^3P_1$ transitions in beryllium Kr XXXIII with incoming charges 31+ and 32+ [Fig. 2(b)]. The ratio of light intensities

$$\frac{I(^3P_0\text{-}^3P_1)}{I(^1S_0\text{-}^1P_1)}$$

for triplet and singlet levels in berylliumlike krypton is found lower when the incoming charge is 32+ than when it is 31+. More precisely this ratio grows from less than 2 up to 4 when the incoming charge changes from 32+ to 31+ with carbon foil of about 100 $\mu g/cm^2$. It appears that it is easier to obtain triplet states of ion with charge state q from an incident beam of charge $q-1$ than from an incident beam of charge q. This can be interpreted as an effect of spin conservation during the collision in an electric dipole excitation. When using a thin carbon foil (5–10 $\mu g/cm^2$) fulfilling the single collision conditions, pure spectra can be obtained and clear spectroscopy can be performed.

In the same way, a 300-$\mu g/cm^2$ carbon foil has been found to be the more efficient one to produce excited heliumlike Kr^{34+} in the $1s^2 2p\ ^3P_2$ state when using a lithiumlike Kr^{33+} incident beam.

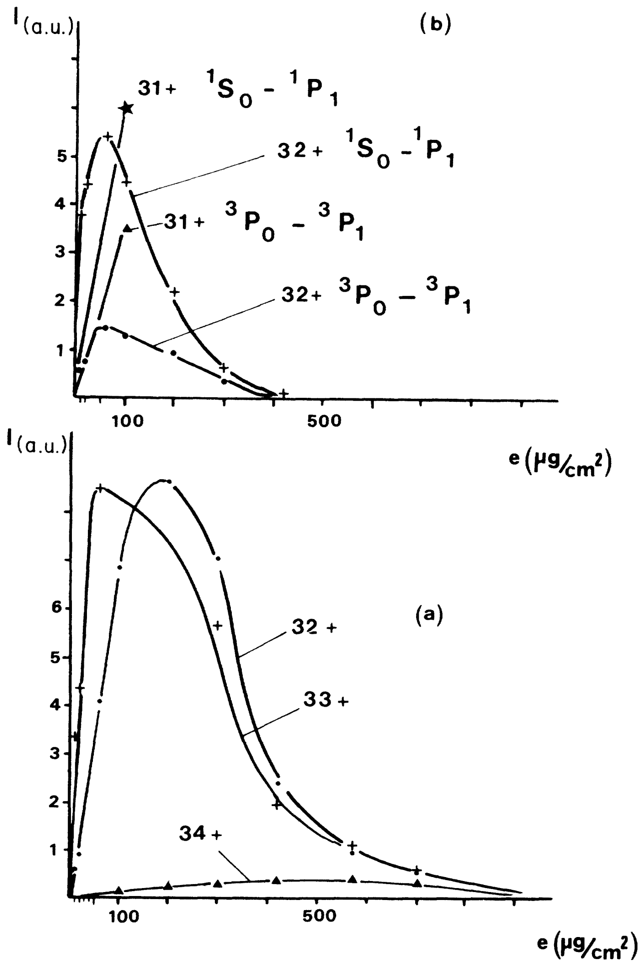

FIG. 2. (a) Kr XXXIV $2s\ ^2S_{1/2}-2p\ ^2P_{3/2}$ intensity emerging from carbon foils with Kr^{32+}, Kr^{33+}, Kr^{34+} ions incident vs foil thickness. (b) $2s^2\ ^1S_0-2s2p\ ^1P_1$ and $2s2p\ ^3P_0-2p^2\ ^3P_1$ transition intensities of 35-MeV/u Kr^{32+} emerging from carbon foils of various thicknesses. Incident charge states are 31+ and 32+.

IV. DATA ANALYSIS

A. Spectra

To take advantage of the selectivity in charge states and, partially, in excited states allowed by use of the LISE facility, several spectra were recorded between 45 and 400 Å. Incident beams were Kr^{26+}, Kr^{27+}, and $Kr^{(30+)-(35+)}$ at 35 MeV/amu. Excitation carbon foil thickness ranged from 5 to 1500 $\mu g/cm^2$. The low-charge spectra obtained from Kr^{26+} and Kr^{27+} and a 5-$\mu g/cm^2$-thick foil have been already analyzed.[12] We present here only highly ionized krypton spectra produced by incoming beams of successive charges $q=30$ to 35.

Typical spectra are displayed in Fig. 3 where we compare line intensities for $q=31,32,33$ and foil thickness 10, 100, and 300 $\mu g/cm^2$, respectively. Each spectrum is the sum of partial spectra placed edge to edge from $\lambda=45$ to 300 Å. Each partial spectrum was obtained for one position of the MCP detector. The spectra were recorded with a 100-μm slit which makes a reasonable resolution of the Kr XXXI–Kr XXXV lines possible. The more intense lines appear in first, second, third, and even fourth orders of diffraction. The lithiumlike $2s\,^2S_{1/2}-2p\ ^2P_{3/2}$ line in Kr XXXIV is very intense in first, second, and third orders with both incident beams Kr^{33+} and Kr^{32+}. The weaker $2s\ ^2S_{1/2}-2p\ ^2P_{1/2}$ line is located in first order near $2s\ ^2S_{1/2}-2p\ ^2P_{3/2}$ in second order. This proximity is favorable to a precise determination of the fine structure. Lines from several charge states are excited in each spectrum: Kr XXXIV and XXXV with incoming Kr^{33+}, Kr XXXIII and XXXIV with incoming Kr^{32+}. Superposition of such lines is possible and has been observed indeed. This is in the case of the transitions $2s\ ^2S_{1/2}-2p\ ^2P_{1/2}$ of Kr XXXIV and $2s\ ^3S_1-2p\ ^3P_2$ of Kr XXXV which are blended by the transitions $n=7$ to $n=8$ and $2s2p\ ^3P_2-2p^2\ ^3P_2$ of Kr XXXIII, respectively (Fig. 3). To eliminate this blending we have to excite the ion beams with a very thin target. An example of spectra obtained is presented in Fig. 3. The incident beam was Kr^{31+}. Most lines are from Kr XXXII. Lithiumlike and berylliumlike lines are very weak.

Let us now look more closely at the lines of interest in heliumlike krypton. With incoming Kr^{33+} and 300-$\mu g/cm^2$ carbon foil, the $2s\ ^3S_1-2p\ ^3P_2$ line in Kr XXXIV appeared to be free of pollution by $2s2p\ ^3P_2-2p^2\ ^3P_2$ in Kr XXXIII as deduced from comparison with a spectrum obtained with a Kr^{32+} incident beam [Figs. 4(a) and 4(b)].

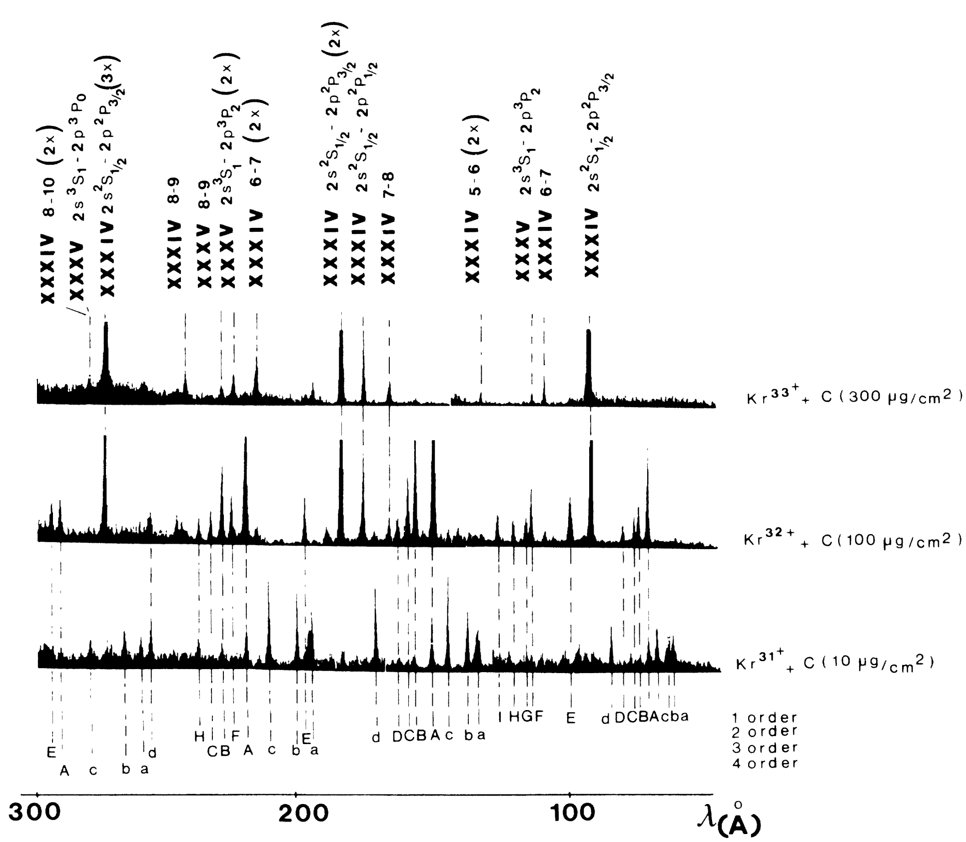

FIG. 3. Krypton spectra obtained between 70 and 300 Å.

Several such spectra with detector position at about 222 Å have been registered for Kr^{33+} incident ions and a 300-$\mu g/cm^2$ foil thickness. Counting time was more than 3 h for one individual recording. Another example is given in Fig. 5 where the $2s\ ^3S_1-2p\ ^3P_2$ line in Kr XXXV is bordered by Rydberg transitions $n=6$ to $n=7$ of Kr XXXIV at second order and $n=8$ to $n=9$ of Kr XXXV at first order. As for the $2s\ ^3S_1-2p\ ^3P_0$ line, only a very long counting time was able to reveal a weak signal at about 280 Å with incident Kr^{33+} beam (Fig. 6). However, a blending with second-order $n=8$ to $n=10$ Kr XXXIV line is not completely excluded. A measurement of the $2p\ ^3P_0$ lifetime was not conclusive due to the weakness of the signal.

B. Results

Wavelengths of lines observed in Be-, B- and C-like krypton using selected incident charges and foil thicknesses are listed in Tables I and II. Results in Kr XXXIII are compared with semiempirical data of Edlen[13] and theoretical values of Cheng, Kim, and Desclaux.[14] The intercombination line $2s^2\ ^1S_0-2s2p\ ^3P_1$ has been previously measured by Dietrich *et al.*[15] using beam-foil spectroscopy and by Denne *et al.*[16] in the Joint European Torus (JET) tokamak source. Results are consistent (Table I). The error bars in fine-structure energies of Table I have been obtained by adding the uncertainties on the optical transition energies. The relative errors are actually much lower than the absolute errors as can be seen by comparing the fine-structure splittings deduced from different couples of transitions: 426 042 and 426 046 cm^{-1} for $2s2p(^3P_2$-$^3P_1)$, 83 312 and 83 308 cm^{-1} for $2p^2(^3P_2$-$^3P_1)$. Our wavelength measurements in boronlike and carbonlike krypton can be compared only to theoretical data of Edlen[17,18] and Cheng, Kim, and Desclaux.[14] Relative intensities observed in Kr XXXI show a good consistency with transition probabilities calculated by Cheng *et al.* (Table II).

Results for heliumlike and lithiumlike krypton are given in Tables III and IV.

The $1s^22s\ ^2S_{1/2}-1s^22p\ ^2P_{3/2,1/2}$ wavelengths and the $1s^22p\ ^2P_{1/2}-^2P_{3/2}$ fine structure are compared to experimental measurements of Dietrich *et al.*[15] and Denne *et al.*[16] (Table III). The slight disagreements will be discussed in Sec. VI. Table IV lists the resultant $1s2s\ ^3S_1-1s2p\ ^3P_{2,0}$ wavelengths of heliumlike kryton. The $1s2s\ ^3S_1-1s2p\ ^3P_2$ experiment involved a total of eight runs, all at 35 MeV/amu, during various counting times. All resulting spectra have been fitted to sums of Gaussian profiles with heights, widths, and centers as parameters. Pollution by the $2s2p\ ^3P_2-2p^2\ ^3P_2$ transition of Kr XXXIII has been found insignificant. Mean-square deviation of the fits is 0.04 Å in second order for the 2s-2p wavelengths as well as for Kr XXXIV, 6→7 and 8→9 and Kr XXXV, 8→9 Rydberg transitions. In these

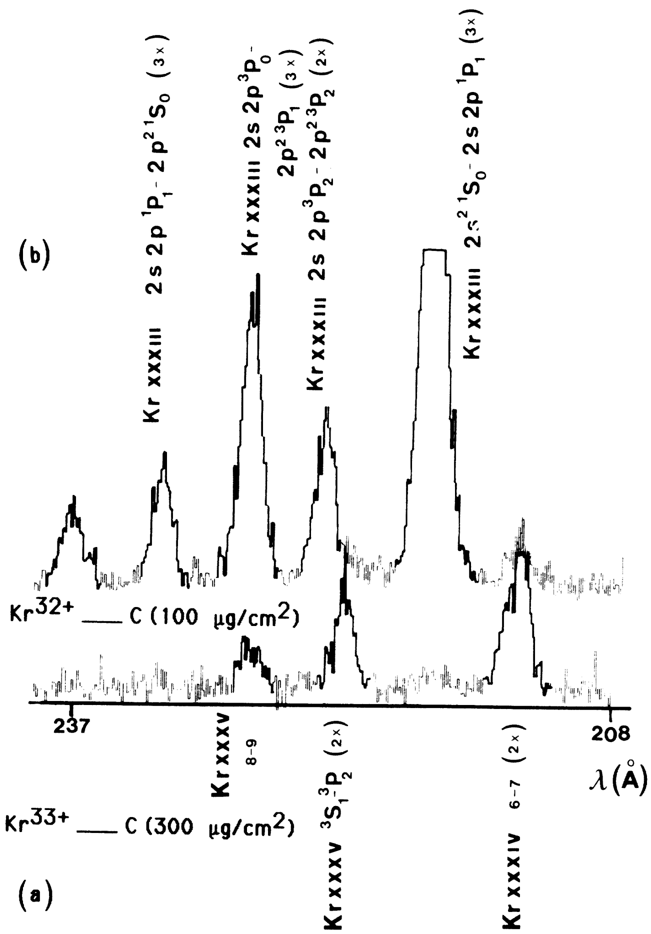

FIG. 4. Krypton spectra between 212 and 238 Å, for incident charge state and foil thickness: (a) 33+, 300 $\mu g/cm^2$ and (b) 32+, 100 $\mu g/cm^2$.

measurements we used for calibration both methods described in Secs II B and II C. The results for the $2s\ ^3S_1-2p\ ^3P_2$ wavelength and 111.121 and 111.101 Å from absolute and Rydberg calibration methods, respectively. The final result is 111.11±0.03 Å. Low statistics of each measurement and inaccuracy in determination of the observation angle are the major contributions to the final uncertainty in $2s\ ^3S_1-2p\ ^3P_2$ measurement. Uncertainty on Rydberg line wavelengths is due to the ignorance of the population distribution and to the "differential" Doppler-Fizeau shift[10] related to the short lifetimes of $n=5$ and 8 levels. Uncertainty on the $2s\ ^3S_1-2p\ ^3P_0$ transition of Kr XXXV is mainly due to statistical errors.

V. WAVELENGTHS OF 2s-2p TRANSITIONS IN TWO-ELECTRON SYSTEMS

A. Calculation of the $1s2s\ ^3S_1-1s2p\ ^3p_2$ transition energy in Kr^{34+}

For high-Z ions, level energies can be calculated using two different methods. Z-expansion calculations have

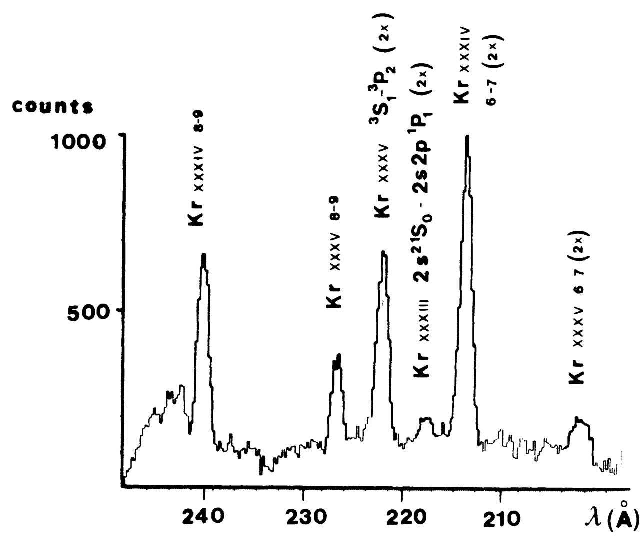

FIG. 5. Spectrum showing the Kr XXXV $2s\ ^3S_1-2p\ ^3P_2$ line (second order) between the Kr XXXV $n=8$ to $n=9$ (first order) and Kr XXXIV $n=6$ to $n=7$ (second order) Rydberg lines.

been performed by DeSerio et al.,[19] Safronova,[20] and Drake.[1] The multiconfigurational Dirac-Fock method has been used by Hata and Grant[21] and by Indelicato, Gorceix, and Desclaux.[3] Theoretical results for Kr XXXV are presented and compared to our measurement in Table V.

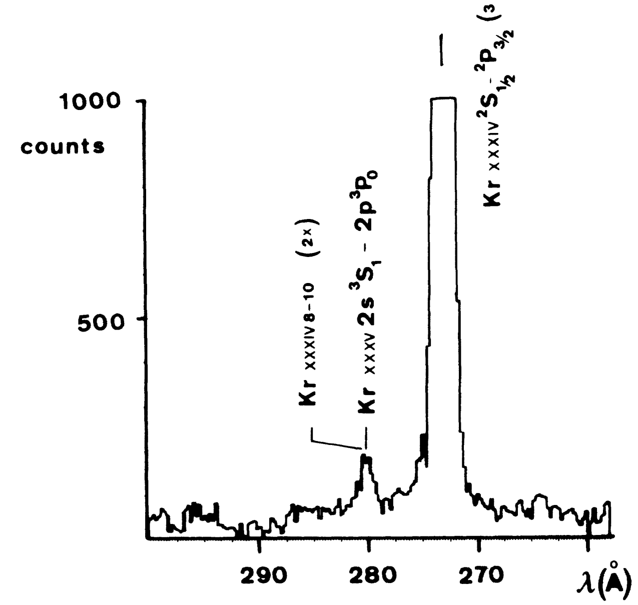

FIG. 6. The Kr XXXV $2s\ ^3S_1-2p\ ^3P_0$ observed near the strong Kr XXXIV $2s_{1/2}-2p_{3/2}$ peak in third order. This helium-like line may be blended with the lithiumlike transition $n=8$ to $n=10$ at second order.

TABLE I. Measured wavelengths (Å) and fine-structure splittings (cm^{-1}) in berylliumlike Kr XXXIII. Comparison with MCDF data, semiempirical prediction and other experimental values in tokamak plasmas. Letters $A, B, \ldots, I$ in the first column refer to those in Fig. 3.

	Transitions	λ (Å) This work	MCDF[a]	Semiempirical[b]	Expt.
			$2s^2$-$2s2p$		
A	$^1S_0$-$^1P_1$	72.66±0.05	72.27	72.65	72.756±0.020[c]
			$2s2p$-$2p^2$		
A	$^3P_2$-$^3D_2$	72.66±0.05	72.19	71.91	
B	$^3P_1$-$^3P_2$	75.66±0.05	75.47	76.28	
B	$^3P_0$-$^3P_1$	75.66±0.05	75.50	75.55	
D	$^3P_1$-$^3P_1$	80.75±0.08	80.67	80.64	
F	$^3P_2$-$^3P_2$	111.65±0.05	110.8	112.93	
H	$^3P_1$-$^3P_0$	117.74±0.10	117.2	117.78	
I	$^3P_2$-$^3P_1$	123.10±0.20	122.4	122.75	
C	$^1P_1$-$^1S_0$	77.10±0.05	77.11	76.97	
E	$^1P_1$-$^1D_2$	98.19±0.10	98.70	97.33	
	$2s^2\,^1S_0-2s2p\,^3P_1$	170.03±0.20	169.80	170.11	169.845±0.025[c] 169.9±0.5[d]

Transition	E (cm^{-1}) This work	Semiempirical	Expt.
$2p^2(^3P_1$-$^3P_0)$	389 060±1950	391 062	
$2p^2(^3P_2$-$^3P_1)$	83 310±1720	70 826	
$2s2p(^3P_1$-$^3P_0)$	83 310±2100	83 373	
$2s2p(^3P_2$-$^3P_1)$	426 040±2550	425 416	424 655±90[c]
$2p^2(^1S_0$-$^1D_2)$	278 580±1900	271 820	
$2s2p(^1P_1$-$^3P_1)$	787 950±1640	788 639	785 687±470[c]

[a]Cheng, Kim, and Desclaux (Ref. 14).
[b]Edlen (Ref. 13).
[c]Denne *et al.* (Ref. 16).
[d]Dietrich *et al.* (Ref. 15).

TABLE II. Wavelengths in boronlike Kr XXXII and in carbon Kr XXXI (Å). Letters $a, \ldots, d$ refer to those in Fig. 3.

	Transitions	λ (Å) This work	Edlen[a]	Cheng *et al.*[b]
		$2s^22p$-$2s2p^2$		
d	$^2P_{3/2}$-$^2D_{5/2}$	84.89±0.05	84.37	84.93
c	$^2P_{1/2}$-$^2D_{3/2}$	69.84±0.05	69.83	69.82
b	$^2P_{1/2}$-$^2S_{1/2}$	66.49±0.05	66.60	66.30
a	$^2P_{3/2}$-$^2P_{1/2}$	65.00±0.2	65.00	64.96
a	$^2P_{3/2}$-$^2P_{3/2}$	64.59±0.2	64.59	64.32
		$2s2p^2$-$2p^3$		
	$^2P_{3/2}$-$^2P_{3/2}$	78.90±0.2	78.48	78.86
	$^2D_{5/2}$-$^2D_{5/2}$	93.75±0.2	94.44	93.48
		$2p^22p^2$-$2s2p^3$		
	$^3P_2$-$^3S_1$	59.79±0.05	59.81	59.64
	$^3P_1$-$^3P_0$	64.14±0.05	64.08	64.35
	$^3P_2$-$^3P_2$	63.00±0.05	63.07	63.04
	$^3P_1$-$^3D_2$	79.45±0.05	79.65	79.88
		$2s2p^3$-$2p^4$		
	$^3P_1$-$^3P_0$	79.45±0.05	80.73	79.65

[a]References 17 and 18.
[b]Reference 14.

The value of Safronova for the total transition energy is 1580 cm^{-1} higher than experiment. In her calculation, an earlier value of the one-electron Lamb shift[22] has been used which now has been corrected,[23] no effect of the second electron on the Lamb shift has been estimated, and, more important, no higher relativistic contributions in $Z_-^2[(\alpha^2Z^2)^7+\cdots]$ have been taken into account.

The result of DeSerio *et al.* includes complete QED contributions. The nonrelativistic terms have been obtained by extrapolating up to $Z=36$ the values given by Accad, Pekeris, and Schiff[24] for $3\le Z\le 10$, which presents a large nuclear charge gap and may induce a large uncertainty. The fine-structure one-electron QED contribution has been taken from Garcia and Mack.[25] It is somewhat different from the best available value given by Mohr.[23] The correction to the two-electron QED has been calculated at lower order, which is only valid for low-charge ions. The more recent results for higher-Z ions have been reported by Indelicato, Gorceix, and Desclaux.[3] They used the MCDF method to treat relativistic effects and correlations efficiently. Result includes

TABLE III. Measured wavelengths λ (Å) and fine-structure splitting E (cm^{-1}) in lithiumlike Kr XXXIV.

Transitions	Present expt.	Other beam-foil Dietrich et al.[a]	Tokamak plasma Denne[b]	Denne et al.[c]
λ ($2s\,^2S_{1/2}-2p\,^2P_{3/2}$)	91.00±0.03	91.08±0.10	91.06±0.02	91.049±0.025
λ ($2s\,^2S_{1/2}-2p\,^2P_{1/2}$)	173.93±0.04	174.15±0.26	174.03±0.03	174.036±0.026
E ($2p\,^2P_{3/2}-2p\,^2P_{1/2}$)	523 957±300	523 718±2060	523 563±340	523 716±390

[a]Reference 15.
[b]Reference 8.
[c]Reference 16.

corrections to two-electron QED, relativistic correlations, and retarded interaction. The second-electron effects on self-energy have been estimated using a new method based upon the Welton picture of the Lamb shift.

Our own calculation uses the MCDF results of Indelicato, Gorceix, and Desclaux except for the value of the one-electron QED which we have taken from Mohr[23] and the corrections to the two-body QED we have calculated in the way we develop in the next section.

B. Calculation of the two-electron QED contributions

We start with the Hata and Grant equation[21] for the J-independent part of the total QED contribution:

$$E_{L,2}=E_{L,2}^{\mathrm{KS}}+\tfrac{4}{3}\alpha^3Z\langle\delta(r_1)+\delta(r_2)\rangle[3\pi(\alpha Z)(\tfrac{427}{384}-\tfrac{1}{2}\ln 2)-\tfrac{3}{4}(\alpha Z)^2\ln^2(\alpha Z)^{-2}+(\alpha Z)^2\ln(\alpha Z)^{-2}(4\ln 2-\tfrac{1}{10}+\tilde{A}_{2,0})-(\alpha Z)^2G_{L,2}(\alpha Z)]\ , \quad (1)$$

where $\tilde{A}_{2,0}$ equals $\frac{1}{9}[24\ln 2-\frac{37}{8}]$ and $3\ln 2-\frac{63}{80}$ for $2s\,^3S$ and $2p\,^3P$ levels, respectively, and $E_{L,2}^{\mathrm{KS}}$ is the Kabir and Salpeter[26] expression for two-electron QED limited to lower diagrams.

The value

$$G_{L,2}(\alpha Z)=\tfrac{4}{3}\pi^2+4+4\ln^2 2 \quad (2)$$

taken by Hata and Grant from Garcia and Mack[25] is valid only for $Z\leq 10$. We have approximated $G(\alpha Z)$ for higher-Z ions by a linear combination of hydrogenic values for the two orbitals $1s2l$. Coefficients are chosen to correctly reproduce the hydrogenic result of the higher-Z limit. We obtain

$$[G_{L,2}(\alpha Z)]_{1s2s}=\tfrac{8}{9}[G_{1s}(\alpha Z)+\tfrac{1}{8}G_{2s}(\alpha Z)]\ ,$$
$$[G_{L,2}(\alpha Z)]_{1s2p}=[G_{1s}(\alpha Z)+\tfrac{1}{8}G_{2p}(\alpha Z)]\ . \quad (3)$$

Fitting Mohr data[23] on relations

$$G(\alpha Z)=Z_1+Z_2(Z\alpha)\ln[(Z\alpha)^{-2}]+Z_3(Z\alpha) \quad (4)$$

we obtain the values of coefficients Z_1, Z_2, and Z_3:

$Z_1=21.2711,\quad Z_2=-3.0501,\quad Z_3=-18.5069$ for G_{1s}

$Z_1=21.2707,\quad Z_2=-1.9605,\quad Z_3=-19.4618$ for $G_{2s1/2}$

$Z_1=-0.1593,\quad Z_2=0.894,\quad Z_3=-1.0862$ for $G_{2p1/2}$.

For the calculation of the electron density at the origin $\langle\delta(r_1)+\delta(r_2)\rangle$, we have used the fit to the values of Accad, Pekeris, and Schiff[24] as made by Hata and Grant[21] and we have considered the increase of relativistic wave function at the origin using the MCDF code of Desclaux.[27] The increase reaches about 20% for krypton.

The vacuum polarization is weak compared to the self-energy. So we did not take account of its higher-order terms which amount only to a few percent of the two-electron QED contribution.

The effect of the second electron on QED is deduced from the total QED contribution, which we have just calculated above, by subtracting the one-electron QED contribution so that

TABLE IV. Measured wavelengths (Å) of $2s\,^3S_1$–$2p\,^3P_2$ and $2s\,^3S_1$–$2p\,^3P_0$ transitions in heliumlike Kr XXXV.

Transitions	Calibration on angle and beam velocity	Calibration on incident-beam Rydberg lines	Resulting wavelengths
$1s2s\,^3S_1-1s2p\,^3P_2$	111.121	111.101	111.11±0.03
$1s2s\,^3S_1-1s2p\,^3P_0$			279.80±0.2

TABLE V. $2s\,^3S_1-2p\,^3P_2$ transition energy (cm^{-1}) in heliumlike Kr XXXV. Comparison between experimental and theoretical data.

Authors	Relativistic and nonrelativistic energy sum	QED contribution First electron	QED contribution Second electron	Resulting energies
DeSerio[a] 1/Z expansion	912 382.1	−12 784.9	432	900 029
Safronova[b] 1/Z expansion	914 064	−12 478		901 586
Indelicato[c] MCDF			380	900 164
This work MCDF	912 467	−12 669	301	900 099
Experiment				900 009(±160)

[a]Reference 19.
[b]Reference 20.
[c]Reference 6.

$$\Delta_{L,2}=\tfrac{4}{3}\alpha^3 Z\langle\delta(r_1,r_2)\rangle\left[\tfrac{19}{30}+\ln\frac{Z^2R}{K_0(1snl)}-2\ln(\alpha Z)+3\pi(\alpha Z)(\tfrac{427}{384}-\tfrac{1}{2}\ln 2)-\tfrac{3}{4}(\alpha Z)^2\ln^2[(\alpha Z)^{-2}]\right.$$
$$\left.+(\alpha Z)^2\ln[(\alpha Z)^{-2}](4\ln 2-\tfrac{1}{10}+\tilde{A}_{2,0})-(\alpha Z)^2 G_{L,2}(\alpha Z)\right], \qquad (5)$$

where $K_0(1snl)$ is the mean excitation energy.

For J-dependent terms, we have to subtract:

$$E_{L,1}(nlj)=\frac{\alpha^3 Z^4(1-\delta_{l,0})C_{l,j}}{2\pi n^3(2l+1)}, \qquad (6)$$

where $C_{l,l+1/2}=(l+1)^{-1}$ and $C_{l,l-1/2}=-l^{-1}$. The corresponding corrections are

$$\Delta E^0_{1,2}=\frac{\alpha^3Z^3}{96\pi}(10.336\,10-12.383\,19/Z),$$
$$\Delta E^1_{1,2}=\frac{\alpha^3Z^3}{96\pi}(2.794\,467-1.750\,19/Z), \qquad (7)$$
$$\Delta E^2_{1,2}=\frac{\alpha^3Z^3}{96\pi}(-3.744\,02+3.526\,75/Z),$$

for the $^3P_0$, $^3P_1$, and $^3P_2$ terms, respectively. Final results for the second-electron effect on QED are

$$\Delta E_{0,2}=\frac{3}{2\pi}(\alpha Z)^3(-2.3317-2\ln(\alpha Z)+7.213\,78(\alpha Z)-(\alpha Z)^2\{\tfrac{3}{4}\ln^2[(\alpha Z)^{-2}]-4.007\,09\ln[(\alpha Z)^{-2}]+G_{1s2s}(\alpha Z)\})$$
$$\times(0.187\,883\,5+0.054\,632/Z+0.016\,471\,5/Z^2)O_{r=0}(1s2s\,^3S_1) \qquad (8)$$

for the $1s2s\,^3S_1$ term, and

$$\Delta E_{1,2}=\frac{4}{3\pi}(\alpha Z)^3\{-2.3471-2\ln(\alpha Z)+7.213\,78(\alpha Z)-(\alpha Z)^2[3/4\ln^2(\alpha Z)^{-2}-3.964\,53\ln(\alpha Z)^{-2}+G_{1s2p}(\alpha Z)]\}$$
$$\times(-0.086\,437+0.128\,566/Z-0.001\,734/Z^2)O_{r=0}(1s2p\,^3P_J) \qquad (9)$$

for the $1s2p\,^3P_J$ term, to which we have to add the J-dependent corrections given by (7). In (8) and (9), $G_{1s2s}(\alpha Z)$ and $G_{1s2p}(\alpha Z)$ are given by (3) and (4) and the $O_{r=0}(1snl)$ are the relativistic corrections to the wave function at the origin.

The calculated second-electron QED contributions to the $1s2s\,^3S_1-1s2p\,^3P_2$ and $1s2s\,^3S_1-1s2p\,^3P_0$ transition energies are presented in Table VI for ions of nuclear charges between 3 and 54. Comparison with theoretical values of Hata and Grant[21] is not directly relevant because of a sign error in the constant multiplying the $(\alpha Z)^2$ term of their relations 3.21 and 3.22 (read

+19.0813 in place of −19.0813). For low-charge ions ($Z \leq 10$) the agreement is not bad but for higher charge ions the differences become significant. For the $1s2s\,^3S_1-1s2p\,^3P_2$ transition in heliumlike krypton, the DeSerio *et al.*[19] extrapolated value of 432 cm^{-1} is significantly higher than our value of 301 cm^{-1} and than the Indelicato, Gorceix, and Desclaux[3] calculation of 380 cm^{-1}.

TABLE VI. Second-electron QED contributions (cm^{-1}) to $2s\,^3S_1-2p\,^3P_2$ and $2s\,^3S_1-2p\,^3P_0$ energies in the helium sequence for $3 \leq Z \leq 54$.

Z	$2s\,^3S_1-2p\,^3P_2$	$2s\,^3S_1-2p\,^3P_0$
3	+0.76	+0.82
4	+1.55	+1.74
5	+2.71	+3.10
6	+4.26	+4.96
7	+6.24	+7.39
8	+8.67	+10.42
9	+11.56	+14.10
10	+14.94	+18.47
11	+18.82	+23.58
12	+23.21	+29.45
13	+28.13	+36.11
14	+33.57	+43.62
15	+39.56	+51.98
16	+46.09	+61.25
17	+53.18	+71.44
18	+60.83	+82.59
19	+69.05	+94.73
20	+77.83	+107.89
21	+87.20	+122.09
22	+97.15	+137.36
23	+107.68	+153.75
24	+118.81	+171.26
25	+130.54	+189.94
26	+142.88	+209.82
27	+155.82	+230.91
28	+169.39	+253.27
29	+183.58	+276.91
30	+198.41	+301.86
31	+213.87	+328.17
32	+229.99	+355.85
33	+246.77	+384.96
34	+264.22	+415.51
35	+282.35	+447.55
36	+301.17	+481.11
37	+320.71	+516.23
38	+340.96	+552.94
39	+361.95	+591.30
40	+383.70	+631.32
41	+406.21	+673.07
42	+429.52	+716.58
43	+453.64	+761.89
44	+478.59	+809.05
45	+504.40	+858.12
46	+531.09	+909.13
47	+558.69	+962.14
48	+587.23	+1017.21
49	+616.75	+1074.38
50	+647.26	+1133.72
51	+678.82	+1195.29
52	+711.45	+1259.14
53	+745.20	+1325.34
54	+780.11	+1393.96

C. Comparison between theory and experiments for $Z \leq 54$

A comparison of experiments with theory for the $^3S_1$-$^3P_2$ transition energy along the helium isoelectronic sequence is shown in Fig. 7 and in Table VII. Previous observed energies are taken from DeSerio *et al.*[19] and Galvez *et al.*[28] Recent precise measurements have been obtained for neon and argon by Beyer, Folkmann, and Schartner[29] and for Mg and Al by Klein *et al.*[30] Theoretical values are split into three terms in Table VII: the non-QED part, the first-electron QED contribution and the second-electron QED correction. The non-QED part is taken from Hata and Grant[21] for $Z \leq 30$ and from Indelicato, Gorceix, and Desclaux[3] for Z=22, 26, 29, 36, and 54. The first-electron QED contribution is from Mohr and the second-electron QED correction is issued from Table VI. Comparison of experiment and theory for the $1s2s\,^3S_1-1s2p\,^3P_2$ transitions is plotted with respect to the experimental values for $3 \leq Z \leq 36$ (Fig. 7). It appears that, for higher Z, the values calculated by Indelicato, Gorceix, and Desclaux are in particularly good agreement with measurements. The importance of the two-electron QED correction is displayed by the dashed curve of Fig. 7.

VI. THE $1s^22s\,^2S_{1/2}-1s^22p\,^2P_{1/2,3/2}$ TRANSITIONS IN THREE-ELECTRON SYSTEMS

Measured and calculated values of the $1s^22s\,^2S_{1/2}-1s^22p\,^2P_{1/2,3/2}$ transition energies and $^2P_{1/2}$-$^2P_{3/2}$ fine structure in Kr XXIV are displayed for comparison in Table III, VIII, and IX. Measurements are available from spectra of fast-ion excitation and tokamak plasmas (Table III). Lower signal-to-noise ratio and lack of lines for calibration due to lower beam energy yield to higher error bars in the beam-foil data of Dietrich *et al.*[15] However, beam-foil results are consistent and are both largely inside the two sets of uncertainty. This is not true when comparing our results with the plasma results. The differences of 724 and 330 cm^{-1} between our values and the measurement of Denne and co-workers,[8,16] for $2s_{1/2}$-$2p_{3/2}$ and $2s_{1/2}$-$2p_{1/2}$ transitions, respectively, could be assumed to be due to Doppler effects. The first- and second-order Doppler shifts, tied to the beam-foil technique, have been determined from measurement of the angle between the ion beam and the observation axis ($\simeq 90°$) and the ion-beam velocity ($\beta \simeq \frac{1}{3}$) as detailed in Sec. II C. The Doppler shift is smaller in plasma experiments because of the weak velocity of ions ($\beta \simeq 10^{-3}$). However, in the experiment of Denne and co-workers at an observation angle of 11°35′, the Doppler shift of several 10^{-2} Å observed during the neutral injection is different for lines emitted in the cold side of the machine than for lines of highly ionized atoms reduced in the center of the hot plasma.

TABLE VII. Comparisons between theory and experiment for the $2s\ ^3S_1-2p\ ^3P_2$ transition in two-electron systems. Energies in cm^{-1}. Experimental values are from DeSerio *et al.* (Ref. 19) and Galvez *et al.* (Ref. 28) unless indicated otherwise.

Z	Nonrelativistic, relativistic, and mass polarization energy sum	QED contributions First-electron (Mohr, Ref. 23)	QED contributions Second-electron (Table VI)	Total energy	Expt. (accuracy)	Theor. minus Expt.
3	18 229.42	−2.02	0.76	18 228.16	18 228.198(1)	−0.038
4	26 872.19	−5.78	1.55	26 867.96	26 867.9(6)	0.06
5	35 440.02	−12.97	2.71	35 429.76	35 429.5(6)	0.26
6	44 042.13	−25.00	4.26	44 021.39	44 021.6(10)	−0.21
7	52 756.02	−43.40	6.24	52 718.86	52 719.5(6)	−0.64
8	61 648.28	−69.84	8.67	61 587.11	61 588.1(15)	−0.99
9	70 791.58	−106.09	11.56	70 697.05	70 700.4(30)	−3.35
10	80 257.08	−153.86	14.94	80 118.16	80 123.7(13)[a]	−5.5
12	100 515.37	−291.69	23.21	100 246.9	100 262.7(6)[b]	−15.8
13	111 501.08	−385.61	28.1	111 143.6	111 156.8(6)[b]	−13.2
14	123 199.89	−499.1	33.57	122 734.3	122 746(3)	−11.6
15	135 735.09	−634.3	39.56	135 140.3	135 153(18)	−12.6
16	149 232.07	−793.0	46.1	148 485.2	148 493(5)	−7.8
17	163 834.42	−977.9	53.2	162 909.7	162 923(6)	−13.3
18	179 691.4	−1190.9	60.8	178 561.3	178 590.56(32)[a]	−28
22	258 933.8	−2370.5	97.1	256 660.4	256 746(46)	−85
				256 783[g]		37
24	310 676.4	−3189.0	118.8	307 607.2	307 350(360)[c]	257
26	372 756.4	−4188.0	142.9	368 711	368 960(125)	−248
				368 838[g]		−122
28		−5387	169.4	441 852[g]	441 950(78)[d]	−98
29	489 511.1	−6075	183.6	483 619.6	483 910(187)[e]	−290
				483 757[g]		−152
36	912 467	−12 669	301.17	900 099[g]	900 009(160)[f]	90
54	3 803 032	−52 090	780.11	3 754 360[g]		

[a]Beyer, Folkmann, and Schartner (Ref. 29).
[b]Klein *et al.* (Ref. 30).
[c]Grandin *et al.* (Ref. 31).
[d]Zacarias *et al.* (Ref. 33).
[e]Buchet *et al.* (Ref. 32).
[f]This work.
[g]Using energy sum without QED contributions of Indelicato, Gorceix, and Desclaux (Ref. 3).

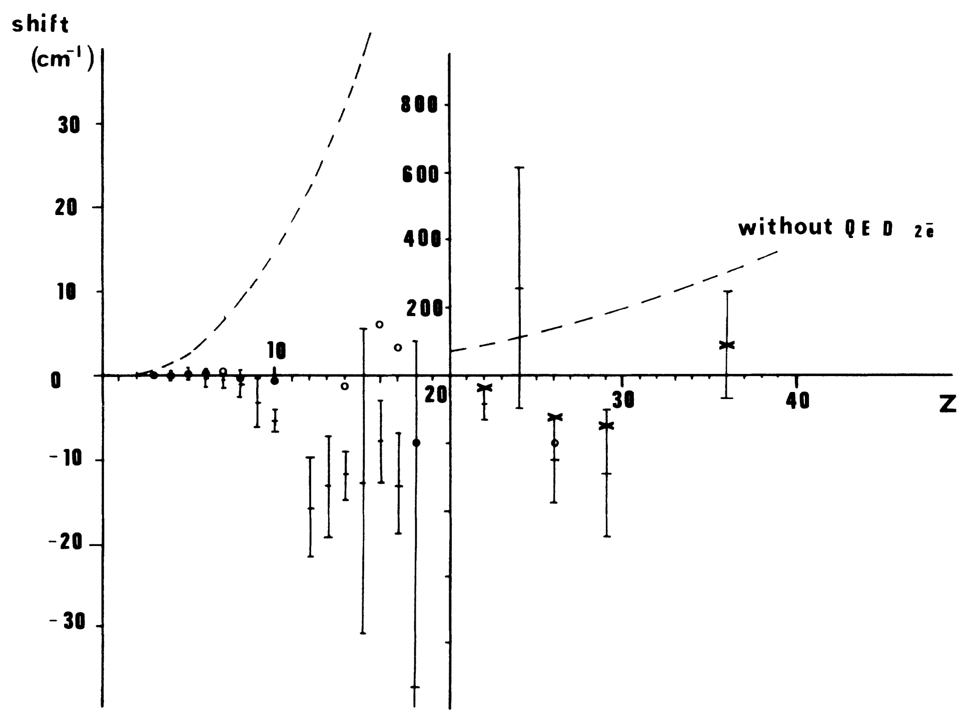

FIG. 7. Comparison of measurements and calculations of the $2s\ ^3S_1-2p\ ^3P_2$ transition energy for heliumlike ions. The theoretical values are from Hata and Grant, +; Goldman and Drake (Ref. 34), ○; Indelicato, Gorceix, and Desclaux (Ref. 3), ×. Dashed curves show what would be differences if the QED contributions were not screened.

TABLE VIII. Comparison between theory and experiment for the energy (cm^{-1}) of the $2s\,^2S_{1/2}$–$2p\,^2P_{3/2}$ transition in Kr XXXIV.

Parameter	Value
MCDF	1 111 302
First-electron QED cont.	−12 669
First-order correlation	−1 207
High-order correlation	+65
E_{theor}	1 097 491
E_{expt}	1 098 900±360
$E_{\mathrm{theor}}-E_{\mathrm{expt}}$	−1 409
E_{theor} (Indelicato)[a]	1 098 293
E_{theor} (Johnson et al., without QED)[b]	1 109 687
E_{theor} (Johnson et al., with first-electron QED)[b]	1 097 336
$E_{\mathrm{semi\,emp.}}$ (Edlen)[c]	1 098 849
E (Curtis)[d]	1 098 273

[a]Reference 6.
[b]Reference 5.
[c]Reference 13.
[d]Reference 35.

TABLE IX. Comparison between theory and experiment for the energy (cm^{-1}) of the $2p\,^2P_{1/2}$–$^2P_{3/2}$ fine structure in Kr XXXIV.

Parameter	Value
MCDF	522 643
First-electron QED cont.	+1 251
Second-electron QED cont.	−160
$\omega\neq 0$ retardation	−397
Relativistic correlation	+221
E_{theor}	523 558
E_{expt}	523 957±300
$E_{\mathrm{theor}}-E_{\mathrm{expt}}$	−399
E_{theor} (Indelicato)[a]	523 566.5
E_{theor} (Johnson et al., without QED)[b]	522 626
E_{theor} (Johnson et al., with first-electron QED)[b]	523 882
$E_{\mathrm{semi\,emp.}}$ (Edlen)[c]	523 712
E (Seely)[d]	523 741

[a]Reference 6.
[b]Reference 5.
[c]Reference 13.
[d]Reference 35.

In our calculation of energies (Tables VIII and IX) we add to the single configuration MCDF value, the one-electron QED from Table VII and the nonrelativistic correlations. For the $2p_{1/2}$-$2p_{3/2}$ fine structure, the $\omega\neq 0$ Breit term and the one-electron QED screening are displayed, showing that they have the same order of magnitude as the experimental uncertainty.

Semiempirical results of Edlen[13] are based on MCDF tables of Cheng, Kim, and Desclaux[14] with Breit correction, Z-independent correlation energy and Lamb shift contributions. In his MCDF calculations Indelicato[6] has included multiconfiguration interactions, retardation contribution, and radiative corrections with self-energy screening in addition to terms appearing in the Cheng, Kim and Desclaux calculations. In their many-body perturbation theory calculation of $n=2$ state energies, Johnson, Blundell, and Sapirstein include the second- and third-order correlation corrections and the lowest-order Breit interaction with retardation. To the values of Johnson, Blundell, and Sapirstein we have added QED corrections from Mohr and screening energies. Then, after these corrections, the MBPT value for energies agrees very well with the value of Indelicato for the $2s_{1/2}$-$2p_{3/2}$ transition but not with $2s_{1/2}$-$2p_{1/2}$ and fine-structure energies. Energies calculated by Johnson, Blundell, and Sapirstein have been combined with QED contributions deduced from an effective screening parameter by Curtis[35] and from a MCDF calculation by Seely.[36]

VII. CONCLUSION

The combination of a selected charge state for the incident ion beam and a thin exciter foil gives the best excitation conditions for the observation of heliumlike and lithiumlike lines, free of contamination from other charge states. We obtain a value for wavelength of the $2s\,^3S_1-2p\,^3P_2$ transition with an accuracy of ±270 ppm which is equivalent to ±2% of the one-electron QED contribution. From the precision of 230 and 330 ppm on the $1s^22s\,^2S_{1/2}-1s^22p\,^2P_{1/2,3/2}$ transitions the fine structure is deduced with an accuracy of 570 ppm. The results obtained are in reasonable agreement with theory but in poor agreement with tokamak plasma measurements in lithiumlike krypton. The more intense ion beam now available at GANIL and a new grating should improve signal intensity and resolution. These advances could result in the realization of a net improvement in wavelength accuracy.

[1]G. W. F. Drake, Can. J. Phys. **66**, 586 (1988).
[2]J. Hata and I. P. Grant, J. Phys. B **17**, 931 (1984).
[3]P. Indelicato, O. Gorceix, and J. P. Desclaux, J. Phys. B **20**, 651 (1987).
[4]I. Lindgren, Phys. Rev. A **31**, 1273 (1985).
[5]W. R. Johnson, S. A. Blundell, and J. Sapirstein, Phys. Rev. A **37**, 2764 (1988); J. Sapirstein, Nucl. Instrum. Method, **31**, 70 (1988).
[6]P. Indelicato, J. Phys. (Paris) Colloq. **12**, C9-297 (1987).
[7]S. Martin, J. P. Buchet, M. C. Buchet-Poulizac, A. Denis, M. Druetta, J. Désesquelles, J. P. Grandin, D. Hennecart, X. Husson, D. Lecler, and I. Lesteven, Phys. Rev. A **35**, 2327

(1987).
[8]B. Denne and E. Hinnov, Phys. Scr. **35**, 811 (1987).
[9]S. Martin, M. Druetta, and J. Désesquelles, Nucl. Instrum. Methods B **14**, 254 (1986).
[10]J. P. Buchet, M. C. Buchet-Poulizac, A. Denis, J. Désesquelles, M. Druetta, E. J. Knystautas, and D. Lecler, Nucl. Instrum. Methods **202**, 79 (1982).
[11]R. Bimbot (private communication).
[12]J. P. Buchet, M. C. Buchet-Poulizac, A. Denis, J. Désesquelles, M. Druetta, S. Martin, D. Lecler, E. Luc Koening, and J. F. Wyart, Nucl. Instrum. Methods B **31**, 177 (1988).
[13]B. Edlen, Phys. Scr. **28**, 51 (1983).
[14]K. T. Cheng, Y. K. Kim, and J. P. Desclaux, At. Data Nucl. Data Tables **24**, 111 (1979).
[15]D. D. Dietrich, J. A. Leavitt, H. Gould, and R. Marrus, Phys. Rev. A **22**, 1109 (1980).
[16]B. Denne, E. Hinnov, J. Ramette, and B. Saoutic, Phys. Rev. A **40**, 1488 (1989); E. Hinnov *et al.*, Phys. Rev. A **40**, 4357 (1989).
[17]B. Edlen, Phys. Scr. **28**, 483 (1983).
[18]B. Edlen, Phys. Scr. **31**, 345 (1985).
[19]R. DeSerio, H. G. Berry, R. L. Brooks, J. Hardis, A. E. Livingston, and S. J. Hinterlong, Phys. Rev. A **24**, 1872 (1981).
[20]U. I. Safronova, Phys. Scr. **23**, 241 (1981).
[21]J. Hata and I. P. Grant, J. Phys. B **16**, 523 (1983).
[22]P. Mohr, Phys. Rev. Lett. **34**, 1050 (1975).
[23]P. Mohr, At. Data Nucl. Data Tables **29**, 453 (1983).
[24]Y. Accad, C. L. Pekeris, and B. Schiff, Phys. Rev. A **4**, 516 (1971).
[25]J. D. Garcia and J. E. Mack, J. Opt. Soc. Am. **55**, 654 (1965).
[26]P. K. Kabir and E. E. Salpeter, Phys. Rev. **108**, 1256 (1957).
[27]J. P. Desclaux, Comput. Phys. Commun. **9**, 31 (1975).
[28]E. J. Galvez, A. E. Livingston, A. J. Mazure, H. G. Berry, L. Engström, J. E. Hardis, L. P. Sommerville, and D. Zei, Phys. Rev. A **33**, 3667 (1986).
[29]H. F. Beyer, F. Folkmann, and K. H. Schartner, Z. Phys. D **1**, 65 (1986).
[30]H. A. Klein, F. Moscatelli, E. G. Myers, E. H. Pinnington, J. D. Silver, and E. Träbert, J. Phys. B **18**, 1483 (1985).
[31]J. P. Grandin, M. Huet, X. Husson, D. Lecler, D. Touvet, J. P. Buchet, M. C. Buchet-Poulizac, A. Denis, J. Désesquelles, and M. Druetta, J. Phys. (Paris) **45**, 1423 (1984).
[32]J. P. Buchet, M. C. Buchet-Poulizac, A. Denis, J. Désesquelles, M. Druetta, J. P. Grandin, X. Husson, D. Lecler, and H. F. Beyer, Nucl. Instrum. Methods B **9**, 645 (1985).
[33]A. S. Zacarias, A. E. Livingston, Y. N. Lu, R. F. Ward, H. G. Berry, and R. W. Dunford, Nucl. Instrum. Methods B **31**, 41 (1988).
[34]S. P. Goldman and G. W. F. Drake, J. Phys. B **17**, L197 (1984).
[35]L. J. Curtis, Phys. Scr. **39**, 447 (1989).
[36]J. F. Seely, Phys. Rev. A **39**, 3682 (1989).